Square Arrays of Vertical Cylinders of PS-*b*-PMMA on Chemically Nanopatterned Surfaces

Sang-Min Park,[†] Gordon S. W. Craig,[†] Young-Hye La,[†] Harun H. Solak,[‡] and Paul F. Nealey*,[†]

Department of Chemical and Biological Engineering and Center for Nanotechnology, University of Wisconsin—Madison, Madison, Wisconsin 53706, and Laboratory for Micro- and Nanotechnology, Paul Scherrer Institut, Villigen/PSI, Switzerland CH-5232

Received January 27, 2007; Revised Manuscript Received May 15, 2007

ABSTRACT: Cylinder-forming polystyrene-*block*-poly(methyl methacrylate) (PS-*b*-PMMA) thin films were directed to assemble on chemically nanopatterned surfaces consisting of a square array of spots with varying diameters of lattice spacing and spot size. In all cases the patterned spots were preferentially wet by the PMMA block in a continuum of surface wet by the PS block. On this chemical pattern, cylindrical domains oriented perpendicular to the surfaces formed a square array of vertical cylinders, instead of a hexagonal array typically formed in the bulk morphology of cylinder-forming block copolymers. When the lattice spacing of chemical spot patterns was incommensurate with the natural dimension of diblock copolymer in a square array, surface reconstruction led to the formation of microdomain structures that do not appear naturally in the bulk state, such as a loop structure of PMMA cylinders connecting two neighboring PMMA cylindrical sections, and semicylinder domains located at the center of the square unit cell, which did not contact the bottom substrate. The chemically nanopatterned surface became ineffective at forming vertical cylinders with a square array when the cylindrical domains were a distance of 1.5 times the bulk cylinder diameter from the patterned surface. The novel morphologies and the variation of morphology with film thickness shed light on the reconstruction of the microphase-separated block copolymer morphology as it equilibrates in the presence of a chemically nanopatterned substrate.

Introduction

Over the past decade interest has grown in the fundamental physics and wealth of technological applications of the domain structure of thin (sub-100 nm) block copolymer films and their use as templates for patterning at the nanoscale. The thin film geometries of these materials typically mirror the thermodynamically preferred morphologies of the bulk copolymer. However, many desirable geometries cannot be achieved readily with the bulk morphologies of block copolymers. Surface reconstruction, the deviation of a block copolymer's bulk morphology as it equilibrates in the presence of a surface, presents an opportunity to generate scientifically interesting and potentially useful morphologies.[1] In this research, we use a cylinder-forming block copolymer to examine surface reconstruction of the copolymer as its vertically oriented cylindrical microdomains are driven by a square array surface pattern to adjust their morphology from the preferred bulk state, a hexagonal array of cylinders, to a square array of cylinders.

Vertically oriented cylinders in thin films of block copolymers have drawn considerable attention on their own right due to a variety of potential applications. Cylindrical microdomains, in contrast to spot patterns from spherical microdomains, provide high aspect ratio features with vertical sidewalls that are readily amenable for subtractive and additive pattern transfer strategies. Thus, thin films with cylindrical microdomains are a natural choice for fabricating densely packed porous templates at the nanoscale.[2−4] Other potential applications of block copolymer thin films with vertically oriented cylinders include the fabrication of MOSFET's,[5] quantum dots,[6] high surface area devices,[7,8] photovoltaic devices,[9] metallic nanodots,[10−12] and magnetic nanowires.[13]

To generate vertically oriented cylinders in block copolymer thin films, strategies typically must be employed to overcome the preference for one of the blocks to wet the substrate and drive the domain structure to be parallel to the substrate. One approach to the formation of vertically oriented cylindrical microdomains is to use a neutral surface, which prefers neither block of the copolymer, to form thermodynamically stable morphologies. Typically, the neutral surfaces are generated by the deposition of random copolymer brushes on the substrates,[14−17] but neutral surfaces have also been generated using self-assembled monolayers[18] or hydrogen passivation.[17] In contrast to these thermodynamically stable morphologies, researchers have shown that a vertical domain structure also can be achieved by kinetically trapping the copolymer in a nonequilibrium state by various means such as proper spin-coating solvent selection[19,20] or solvent swelling.[21] Researchers have also shown that cylindrical domains above T_g will equilibrate parallel to the electric field lines of an electric field applied across the film.[13,22] By cooling the copolymer film below T_g prior to removing the electric field, the cylinders are trapped in a vertical orientation, whereas they would have been in a horizontal orientation if they had been annealed without an electric field. Finally, vertically oriented cylindrical domains have been achieved with semicrystalline block copolymers via directional crystallization[23] or eutectic solidification.[24]

All of the preceding methods result in vertically oriented cylinders, but there is also a technological need for the vertically oriented cylinders to have long-range order.[4,25,26] Several techniques have been used to generate long-range order of vertically oriented cylinders including solvent annealing,[26−28] thermal annealing,[25] and directional matching of simultaneous crystallization and microphase separation.[23] Graphoepitaxy has

* To whom correspondence should be addressed: e-mail nealey@engr.wisc.edu; Tel 608-265-8171; Fax 608-262-5434.
[†] University of Wisconsin—Madison.
[‡] Paul Scherrer Institut.

10.1021/ma0702344 CCC: $37.00
Published on Web 06/15/2007

become one of the more technologically important methods for generating long-range-ordered, vertically aligned cylindrical domains.[4,5,18,29−31] Finally, the use of chemically nanopatterned surfaces has created the ability to achieve registration of long-range-ordered, vertically aligned lamellar structures,[32] and Monte Carlo simulations have predicted that the use of chemically nanopatterned surfaces should also result in long-range-ordered vertical cylinders.[33]

The preceding work relies on making patterns that match the hexagonal packing of cylindrical domains of the bulk copolymer. However, many potential applications of block copolymer thin films would be hindered if they could only use geometries in the bulk. For example, it would be beneficial to be able to generate a square array of spots, which is one of the canonical structures for microlithographic applications as defined by the Semiconductor Industry Association (SIA).[34] A square array of spots is a desired feature by SIA for a variety of reasons, including that a square array of spots would generate a square of array of vias, which more readily provides an integrated circuit design architecture for addressability and transistor interconnection. One possible route to generating different geometries than those that occur naturally in the bulk would involve reconstruction of the polymer morphology at a surface.

Surface reconstruction of block copolymers on chemically homogeneous surfaces has led to a variety of morphologies not readily obtainable by other means. Lamella-forming block copolymers in thin films can form an array of structures, including lamellar bends, disclinations, and missing rows.[35,36] For cylinder-forming copolymers, an even greater array of morphologies have been observed, including lamella, spheres, perforated lamella, and perpendicular and parallel cylinders as well as combinations of these structures.[37] The evolution of these structures has been studied with in-situ scanning force microscopy,[38] layered imaging,[39] and cross-section imaging.[40] Phase diagrams of some of these morphologies point to the importance of film thickness on the surface reconstruction morphology achieved with cylinder-forming block copolymers.[1,41]

We have previously explored the surface reconstruction of block copolymers as they equilibrate on chemically heterogeneous (or patterned) surfaces.[32] In that work we have shown that the same molecular weight block copolymer will form lamellae of different dimensions as it equilibrates in the presence of chemically nanopatterned surfaces of varying pattern spacings, with a mismatch of the obtained lamellar spacing vs the bulk lamellar spacing of as much as 10%. Other research found that scientifically interesting and potentially useful tortuous morphologies, never before observed in the bulk copolymer, were created when a block copolymer was forced to equilibrate on a surface pattern that had a spacing period that was completely mismatched with that of the copolymer morphology.[42] An examination of the morphologies created when the underlying chemical nanopattern has an intermediate geometry, between a perfect match of the bulk copolymer morphology and a complete mismatch of the bulk morphology, should shed light on surface reconstruction of block copolymers as well as point the way toward useful three-dimensional structures. Here we examine the morphologies created when the substrate pattern is somewhat mismatched from the thermodynamically preferred bulk copolymer morphology, in terms of both spacing and pattern configuration. Specifically, we examine the effects of forcing a hexagonally arranged series of cylinders to equilibrate on a chemical nanopattern consisting of a square array of spots.

Experimental Section

Materials. The primary materials used in this research were the cylinder-forming polystyrene-*block*-poly(methyl methacrylate) block copolymer (PS-*b*-PMMA), the poly(methyl methacrylate) (PMMA) photoresist, and the polymer brush. The PS-*b*-PMMA block copolymer (M_n: 146.7 kg/mol for PS and 70.7 kg/mol for PMMA, PDI = 1.11, purchased from Polymer Source Inc.) was selected because 70 vol % PS results in a cylindrical microphase-separated morphology, in which the PMMA block typically forms a hexagonal array of cylinders. The PMMA resist used for extreme ultraviolet interference lithography (EUV-IL) had a M_n of 950 kg/mol and was purchased from Microchem Corp. For the polymer brush we used a hydroxy-terminated polystyrene (PS) homopolymer (M_n = 9.5 kg/mol, PDI = 1.04) purchased from Polymer Source, Inc. For the sake of comparison with an unpatterned, neutral polymer brush that favored neither PS nor PMMA in the block copolymer, one experiment used a hydroxy-terminated PS-*r*-PMMA random copolymer with 58 vol % PS, which was synthesized by nitroxide-mediated living free-radical polymerization using a hydroxy-terminated 2,2,6,6-tetramethylpiperidin-1-yl oxide (TEMPO)-based initiator.[43,44] Both the PS brush and the PMMA resist have been used in previous research to generate chemically nanopatterned substrates.[32,45−47]

Sample Preparation. The general process for directed assembly of block copolymers on chemically nanopatterned substrates has been previously demonstrated.[42] The PS brush coating on the wafer was generated in the following manner. The PS brush homopolymer was spin-coated from a 1.5 wt % solution in toluene onto a freshly cleaned silicon substrate to yield a 40 nm thick film. The film was subsequently annealed under vacuum for 48 h at 160 °C to react the terminal hydroxyl group on the PS with the native oxide on the surface of the silicon wafer, thereby chemically grafting some of the PS to the silicon wafer. Ungrafted, hydroxy-terminated polystyrene was removed by repeated ultrasonication in toluene for 3 min at 40 °C, yielding an ∼7 nm brush layer of polystyrene on the silicon.

The patterning of the PS brush started with spin-coating the PMMA from 1.2 wt % solution in chlorobenzene to yield a 60 nm thick photoresist film. The coated substrate was baked for 120 s at 130 °C to remove residual solvent. The photoresist was then patterned using the four-beam EUV-IL at the X-ray interference lithography beamline of the Swiss Light Source. The beamline used undulator light with a central wavelength of 13.4 nm, 92 eV, and 4% spectral bandwidth. The exposure dose from the EUV-IL system ranged 50 to 315 mJ/cm^2, with the larger dose yielding larger patterned spot diameters. The mask was made from a semitransparent silicon nitride membrane and consisted of a series of lines and spaces.[48] The resulting pattern in the PMMA photoresist was a square array of spots with varying lattice spacings (L_{sq}) and spot diameters (d_{sq}) in the area of 50 μm by 50 μm. The developing of the exposed photoresist was performed by submerging the patterned photoresist in a 1:3 mixture of methyl isobutyl ketone and isopropyl alcohol for 30 s, rinsing with isopropyl alcohol, and drying in a stream of nitrogen.

An oxygen plasma was used to chemically pattern the PS brush layer through the openings in the PMMA. The plasma was generated in a plasma etch system (PE-200, Plasma Etch, Inc.) running at 100 W with an O_2 flow rate of 8 cm^3/min. The duration of the plasma was 10 s. The brief duration of the plasma removes only ca. 2.4 nm of the exposed PS and chemically modifies the remaining exposed PS, such that it is oxygen-rich and highly polar. The PS brush covered by the photoresist was left unmodified. The remaining photoresist was removed by ultrasonication in warm toluene, resulting in a chemically nanopatterned surface with a square array of spots.

Once the chemical nanopatterning of the PS brush layer was complete, the PS-*b*-PMMA was spin-coated onto it from toluene solutions with copolymer concentrations ranging from 0.8 to 2.0 wt %. Spin speed and spin-coating solution concentration were varied to yield spin-coated films that ranged in thickness from 22

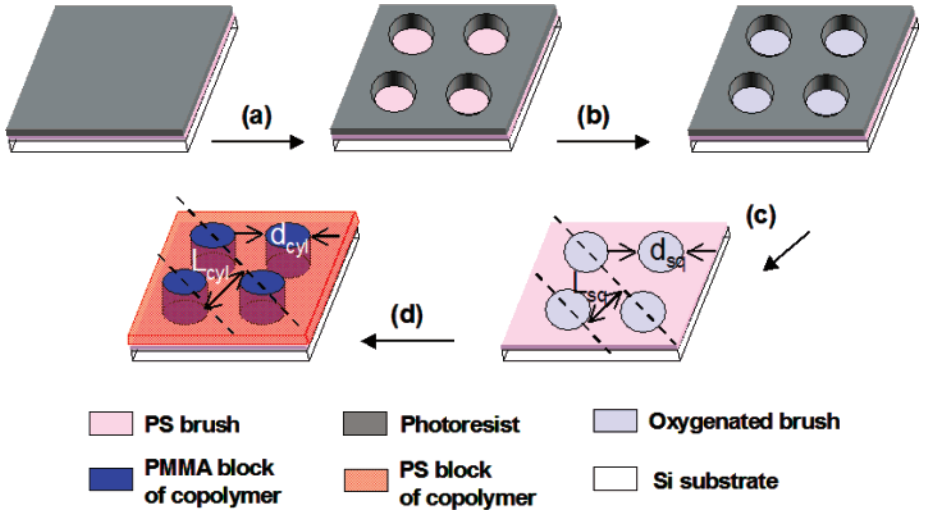

Figure 1. Schematic representation of the strategy used to direct the assembly of cylinders perpendicular to the substrates in registration with the underlying spot patterns with a square array. (a) A photoresist on polystyrene brush layer is patterned with a square array of spots using EUV-IL. The diameter of spot pattern becomes larger as the exposure time is increased. (b) Oxygen plasma treatment is performed to fabricate the chemical nanopattern onto the brush layer. (c) The photoresist is removed. The diameter of spot pattern is d_{sq}, and the lattice spacing of chemical pattern is L_{sq}. (d) The chemically nanopatterned surface is coated with cylinder-forming diblock copolymer thin film and then annealed. The diameter of vertical cylinder is d_{cyl}, and the lattice spacing is L_{cyl}.

to 73 nm. The films were annealed under vacuum at 190 °C for 168 h to permit the thermodynamically preferred morphologies to form.

Analytical Techniques. The film thickness was verified by ellipsometry (Rudolph Research AutoEL-II). The resulting morphologies were imaged using a field emission scanning electron microscope (FESEM) (LEO-1550 VP) under the acceleration voltage of 1 kV without any metal deposition. PMMA resist samples were coated with a thin layer of gold to prevent the deformation of the PMMA by electron beam irradiation during SEM inspection. When it was necessary to improve the contrast in SEM images, the PMMA block was selectively removed by UV irradiation (1 mJ/cm^2) and developed in 97% acetic acid.[3] Image analysis was accomplished by both fast Fourier transform (FFT) and manual optical analysis. The FFT program used was Scion image beta 4.03 from Scion Corp. Atomic force microscopy (AFM) measurements were performed using a Nanoscope III MultiMode AFM from Digital Instruments in the tapping mode. A triangular cantilever made of silicon was used (MikroMasch) in the AFM.

Results

An overview of the directed assembly process, as it applies to the case of cylindrical morphologies, is shown in Figure 1. The PS brush is patterned with EUV-IL and then treated with an oxygen plasma to generate a chemical nanopattern consisting of spots of diameter d_{sq} in a lattice with spacing L_{sq}. The plasma-treated PS surface prefers being coated by the PMMA block of the copolymer whereas the untreated regions have an affinity for the PS block of the copolymer. The chemically nanopatterned surface is spin-coated with a thin cylinder-forming diblock copolymer film and then annealed. The average diameter of resulting vertical cylinders is d_{cyl}, and the lattice spacing is L_{cyl}.

The chemical nanopatterning was inferred from the observed patterning of the PMMA resist. Figure 2 shows the SEM images of spot-patterns printed in a photoresist as a function of L_{sq} (L_{sq} = 50, 60, 70, and 80 nm) and exposure dose. Each image corresponds to a 0.5 μm by 0.5 μm area. The dark region indicates patterned holes, and the bright region indicates remaining photoresist. The diameters of the holes, d_{sq}, depend on the exposure dose so that higher dose provides the larger d_{sq}. In each pattern, the size and shape of the hole patterns are

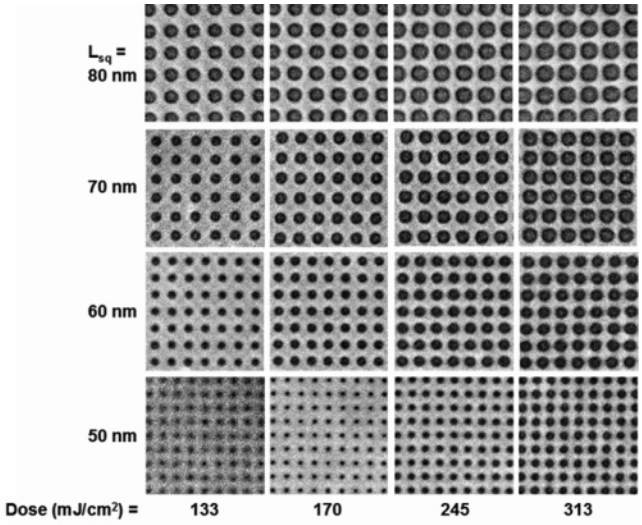

Figure 2. Top-down SEM images of patterned photoresist by EUV-IL with various L_{sq} and doses. The diameters of spots, d_{sq}, become larger as the dose is increased.

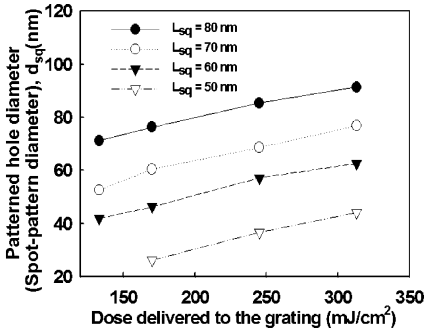

Figure 3. Plot of the patterned surface spot diameters of various L_{sq} vs patterning dose. d_{sq} linearly increases with the increment of dose. Minimum size of d_{sq} is 26.2 nm in L_{sq} = 50 nm, and maximum size of d_{sq} is 91.3 nm in L_{sq} = 80 nm.

quite uniform and regular over a large area. The left-bottom image (L_{sq} = 50 nm, lowest exposure dose) exhibits blurry spots because of the under exposure. Figure 3 shows a plot of d_{sq} for various L_{sq} vs patterning dose for fabricating patterns used in

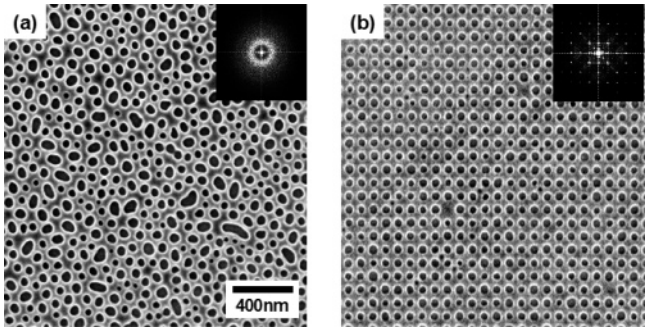

Figure 4. Vertically oriented cylinders of asymmetric PS-*b*-PMMA and 2D fast Fourier transform images (inset) on (a) the flat neutral surface and (b) a square array of spot patterns. A square array of cylinders in 22 nm thick films is directly self-assembled on the chemically nanopatterned spots with $L_{sq} = 60$ nm after annealing for 168 h at 190 °C.

Figure 2. The exposure dose in the graph is the measured dose delivered to the EUV gratings. An increase of exposure dose generates a larger hole size, and furthermore, the formation of larger hole size is favorable in the larger L_{sq} at the same exposure dose. The smallest hole diameter, 26.2 nm, appeared in $L_{sq} =$ 50 nm at 170 mJ/cm^2, and the largest hole diameter, 91.3 nm, appeared in $L_{sq} = 80$ nm at 313 mJ/cm^2. Subsequent stripping of the resist left a polymer brush film that was ~7 nm thick, as determined by ellipsometry. The polymer brush then could be spin-coated with PS-*b*-PMMA, yielding uniform copolymer films with thicknesses in the range of 22−73 nm.

The difference in morphology of block copolymer films spin-coated on the chemically nanopatterned PS brush vs those spin-coated on the neutral PS-*r*-PMMA brush is shown in Figure 4. Figure 4a shows vertically oriented cylinders of PS-*b*-PMMA on the neutral polymer brush surface, and Figure 4b shows the same PS-*b*-PMMA on a square array of spots. In both cases, the PS-*b*-PMMA thin films self-assembled into perpendicularly oriented cylinders of minor block (PMMA) surrounded by the matrix block (PS). On the neutral surface, the cylinders possessed irregular shape and diameters, with a range of diameters from 16 to 89 nm and a standard deviation of 12.8 nm. Hexagonally packed cylinders were rare even over short-range order. Despite the lack of long-range order in the cylindrical microdomains, vertical cylinders of diblock copolymers in thin films typically form hexagonally close packed arrays on the neutral surfaces.[17] However, because of the kinetic limitations inherent in the high-M_n PS-*b*-PMMA, the polymer chains were easily trapped in a nonequilibrium state, resulting in a nonuniform size of cylindrical domains and a loss of lateral ordering of vertical cylinders, as has been seen before with vertical cylinders with high M_n copolymers.[5,17,49] Nonetheless, we were able to use FFT to determine that the average intercylinder distance was 88 nm and the average cylinder diameter (d_{hex}) was 45 nm. We used the intercylinder distance to calculate that the lattice spacing of a hexagonal array (L_{hex}) of PS-*b*-PMMA was 76 nm.

The square array of cylinders formed on the chemically nanopatterned substrate, shown in Figure 4b, was in stark contrast with the disordered aggregate of cylinders shown in Figure 4a. The cylinders in the copolymer film on the chemically patterned substrate formed square arrays of vertical cylinders over arbitrarily large areas. The FFT image shown in the inset of Figure 4b exhibits narrow sharp peaks with a square array, indicating that the vertical cylinders assembled in registration with the underlying chemical pattern. The average diameter of the PMMA cylinders, determined by analysis of the SEM image, was ca. 45 nm with a standard deviation of 6.9 nm and a total range of 30−52 nm. The average diameter was almost equal to the average diameter of the cylinder domains on the neutral surface, but the range and the standard deviation were significantly smaller than the corresponding values for the copolymer on the neutral surface. The average diameter on the chemical nanopattern was also smaller than that of underlying spot patterns. The average diameter d_{sq} and lattice spacing of spot patterns L_{sq} used for this sample were 62.7 and 60.0 nm, respectively.

The effect of varying the patterned spot size d_{sq} while holding the lattice spacing L_{sq} constant is shown in Figure 5. For this series of samples, L_{sq} was 70 nm and d_{sq} was 52.6, 60.5, 68.6, or 76.8 nm. In these samples, some of the square array unit cells had an extra cylinder of PMMA in their center, similar to the fifth spot on a playing die. We refer to this fifth spot as a "semicylinder" because it extends only part of the way from the top surface to the substrate. For all four samples, the sizes of the cylinders and semicylinders were relatively constant, as shown in Figure 5e, and had average diameters of about 45 and 23 nm, respectively. In contrast, the number of semicylinders was strongly dependent on d_{sq}. When the diameter of spot pattern was 52.6 nm, the number of semicylinders was about 30 within a 10 by 10 array of spots of the underlying chemical pattern. The number of semicylinders decreased to about 5 when d_{sq} was 76.8 nm.

We observed semicylinders and another structure in the PMMA phase, which we refer to as "loop cylinders", in the SEM's of 22 nm thick films block copolymer in which L_{sq} was varied from 50 to 80 nm, in 10 nm increments, while keeping the surface spot size constant at $d_{sq} = d_{hex} = 45$ nm, as shown in Figure 6. For all values of L_{sq}, vertical cylinders were obtained. When L_{sq} was 50−60 nm, these cylinders were arranged in a square array with long-range order. When L_{sq} equaled 50 nm, loop cylinders appeared. As L_{sq} increased from 60 to 70 nm, loop cylinders no longer appeared, but semicylinders were present. Both semicylinders and loop cylinders were present when L_{sq} equaled 80 nm, as shown in Figure 6d. We added red circles to Figure 6d to denote the location of the underlying chemical nanopattern to help to show that some of the loop cylinders ran diagonally across a unit cell of the array of the sample with $L_{sq} = 80$ nm, in contrast to the loop cylinders in the sample with $L_{sq} = 50$ nm, which only ran along the grid of the square array. As L_{sq} was increased to 60 nm and beyond, the diameter and number of semicylinders in a 10 by 10 grid of patterned spots increased with increasing L_{sq}, as shown in Figure 6e. Although the semicylinder diameter increased with increasing L_{sq}, the PMMA cylinders on the chemical spot patterns of square arrays maintained the average bulk cylinder diameter L_{hex} of the PS-*b*-PMMA (ca. 45.0 nm) regardless of varying L_{sq}, with the exception of the sample with $L_{sq} = 50$ nm.

To determine the structure of the loop cylinders and semicylinders of the PMMA phase, we used AFM to map the PS matrix surface after the PMMA block was removed, as shown in Figure 7. Figure 7a shows the AFM image and depth profile for a sample containing loop cylinders. Where loop cylinders were present in the film, the opening in the PS left by the removed PMMA descended all the way to the substrate if it was above a patterned, oxidized region of the polymer brush. However, a thin layer was present on top of the substrate between two spot patterns bridged by the loop cylinder. This layer was composed of the PS block because it always wets the PS brush layer in the matrix region of the chemical

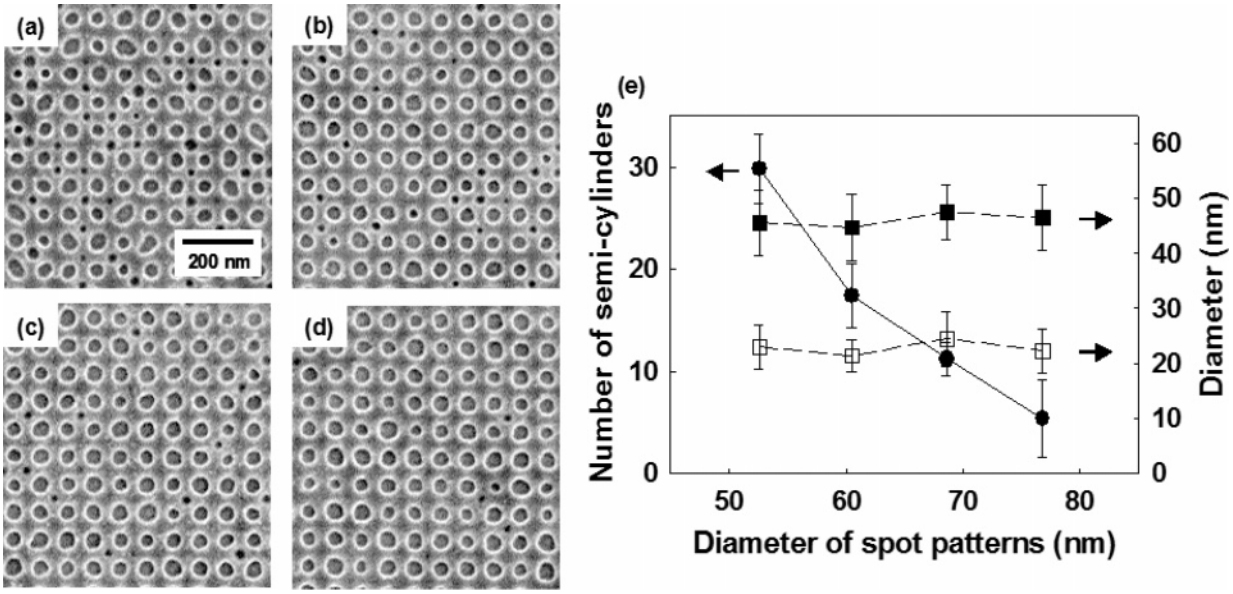

Figure 5. SEM images of directly assembled PS-*b*-PMMA thin film on the chemical spot patterns with various diameters of spot patterns (d_{sq} = (a) 52.6 nm, (b) 60.5 nm, (c) 68.6 nm, and (d) 76.8 nm) and with L_{sq} constant at 70 nm. (e) Plot of (●) average number of semicylinders within 10 by 10 spots of underlying chemical pattern and average diameter of (■) cylinders and (□) semicylinders with varying pattern diameters. The number of semicylinders decreases as the pattern diameter is increased while the diameters of semicylinders and cylinders are not changed.

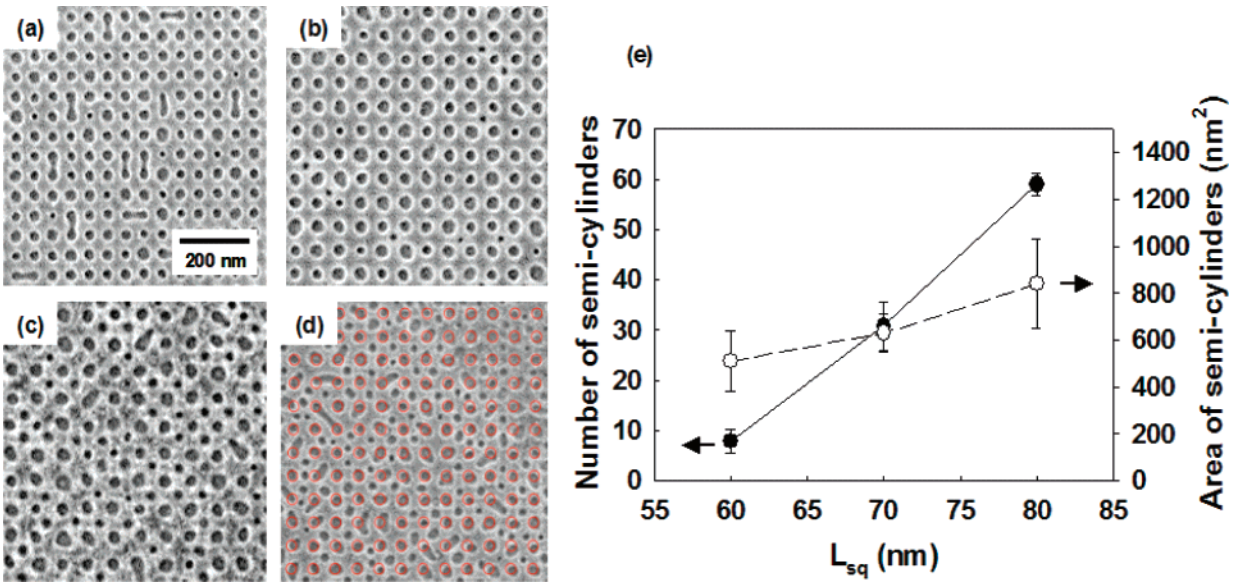

Figure 6. SEM images of directly assembled PS-*b*-PMMA thin film on the chemical spot patterns with various L_{sq} (L_{sq} = (a) 50 nm, (b) 60 nm, (c) 70 nm, and (d) 80 nm) and with d_{sq} = 45 nm. Red circles in (d) represent underlying chemical nanopattern array. Unprecedented morphologies are spontaneously formed by changing L_{sq}. (e) Plot of (●) average number of semicylinders within 10 by 10 spots of underlying chemical pattern and (○) average area of interstitial spots with varying L_{sq}. The number and size of semicylinders formed in the center of a square unit of cylinders increases as L_{sq} increases.

nanopattern, as shown in previous work.[42,50,51] The AFM results for the semicylinders, shown in Figure 7b, were analogous in that AFM detected a thin PS layer that separated the PMMA semicylinders from the substrate. The cylinders above the substrate spot pattern penetrated through the entire film thickness, but the semicylinders had a depth that was less than the depth of the cylinders, even when taking AFM tip convolution effects into account.

We explored the effect of film thickness on the reconstruction of the bulk copolymer structure by preparing 22, 34, 53, and 73 nm thick films of PS-*b*-PMMA on chemically patterned surfaces of a square array with L_{sq} = 60 nm and d_{sq} = 63 nm, as shown in Figure 8a−d. After annealing, 22 nm films produced uniform sized vertical cylinders with square arrays over a large area and had semicylinders in the center of some of the square array unit cells, as shown in Figure 8a. Even though the 34 nm films maintained a square array of cylinders, some of the cylinders appeared as hazy dark spots, which we believe were not fully developed cylindrical domains. In addition to the hazy dark spots, features that looked like either loop cylinders or cylinders parallel with the free surface were present in the 34 nm films. The 53 nm thick films exhibited nonuniformity of the cylinder size as well as more of the loop cylinders or parallel cylinders observed in the 34 nm sample. Finally, at a film thickness of 73 nm, square arrays of cylinders were not observed. As shown in Figure 8d, in the 73 nm thick films, there was a prevalence of cylinders parallel to the surface and nonuniform cylinders. Additionally, localized sections of hex-

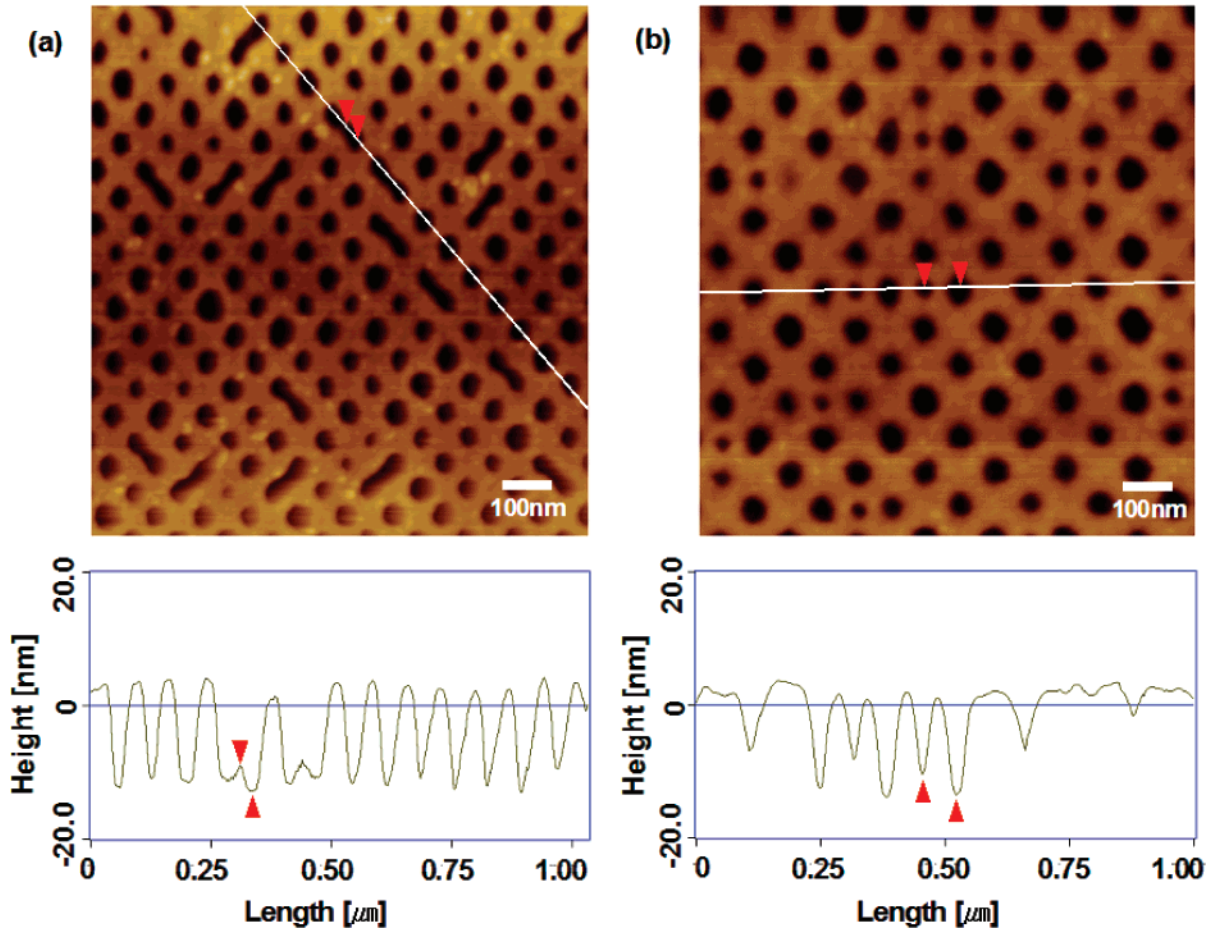

Figure 7. AFM height images of PS matrix assembled on chemical spot patterns of (a) $L_{sq} = 50$ nm and (b) 70 nm after removal of PMMA block selectively and height profiles along the line on the AFM images. All images are rotated by 45°. A thin PS layer exists under the semicylinders and the bridge of the loop cylinders.

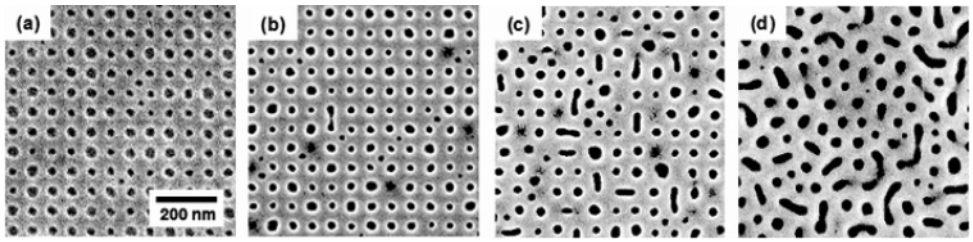

Figure 8. Directly assembled cylinder-forming PS-*b*-PMMA thin films with varying thickness on a chemically patterned square array of spots with $L_{sq} = 60$ nm and $d_{sq} = 63$ nm ((a) 22 nm, (b) 34 nm, (c) 53 nm, and (d) 73 nm thick films). The chemical nanopattern becomes less effective in directing the copolymer morphology as the film thickness is increased.

agonal arrays of vertical cylinders, the thermodynamically preferred bulk structure, were also observed.

The change of cylinder order with varying film thickness was confirmed by azimuthally averaged power spectra of 2D-FFTs of SEM images in Figure 8. Figure 9 exhibits the spectra for each thickness of cylinder-forming PS-*b*-PMMA films assembled on the nanopatterned chemical surface. The 22 nm thick film exhibited narrow sharp peaks at the position of $1:\sqrt{2}:\sqrt{4}:\sqrt{5}$ relative to that of the first-order peak, indicating that PS-*b*-PMMA forms a square array of vertical cylinders on the chemical patterns. For the 73 nm thick film, however, the $\sqrt{2}$, $\sqrt{4}$, and $\sqrt{5}$ peaks were not observed. Additionally, the q value corresponding to the maximum of first-order peak was slightly shifted to the left due to the presence of parallel cylindrical domains at the free surface of films. Therefore, the film thickness of diblock copolymer is critical to maintain the structure of two-dimensional chemical patterns in this work.

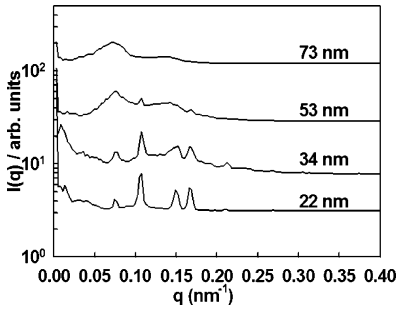

Figure 9. Azimuthally averaged 2D-FFT spectra of the SEM images presented in Figure 8a−d of directly assembled cylinder-forming PS-*b*-PMMA thin films with varying thicknesses on the chemical patterns of square array spots with $L_{sq} = 60$ nm and $d_{sq} = 63$ nm.

The kinetics of the polymer morphology can be observed in Figure 10, which shows the effect of various 190 °C annealing times on the morphology of a series of 22 nm thick films of

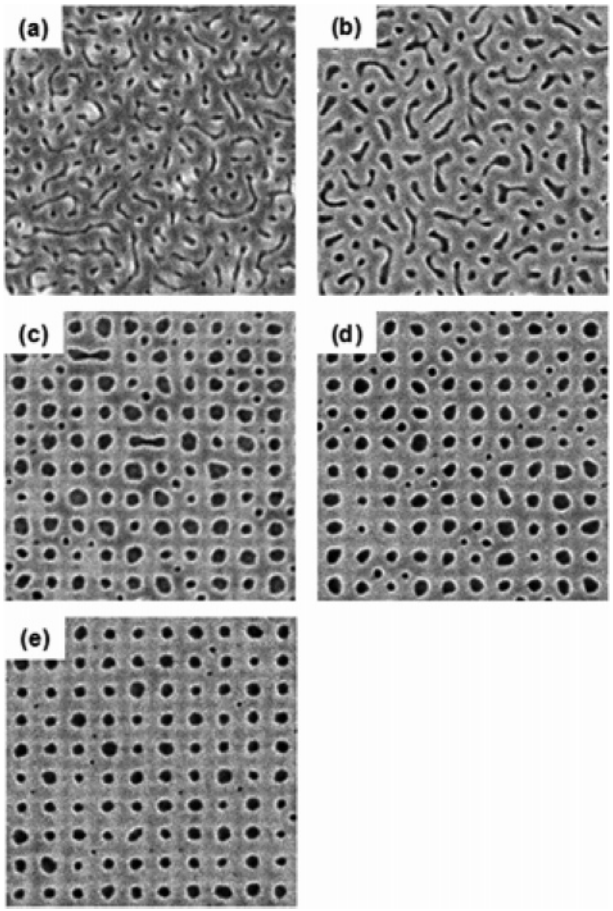

Figure 10. SEM images of cylinder-forming PS-*b*-PMMA on chemical spot pattern of $L_{sq} = 70$ nm and $d_{sq} = 63$ nm, annealed at 190 °C for various times (a) 0 h, (b) 10 min, (c) 2 h, (d) 14 h, and (e) 48 h. Perpendicularly oriented cylinders are formed within 2 h, and well-registered morphology is accomplished for 48 h.

PS-*b*-PMMA on surfaces with $L_{sq} = 70$ nm and $d_{sq} = 60.5$ nm. After spin-coating, the PS and PMMA phases were already segregated on the free surface, as shown in Figure 10a. The cylindrical structure was randomly oriented, and a square array was not developed due to the fast evaporation of solvent during spin-coating. After 10 min annealing, the PMMA phase coalesced so that the size of PMMA domains began to approach the equilibrium value, but the domains were not registered with the underlying chemically spot-patterned substrates. Annealing for 2 h generated a large improvement of the orientation and registration of cylindrical domains with respect to a square array of chemical spot patterns. Perpendicularly oriented cylinders in a square array were clearly visible over a large area, although cylinder size and shape were not quite uniform. The ratio of standard deviation (σ) to the mean diameter (d_{cyl}) of the cylinder size distribution was 0.240. When the film was annealed for 14 h, σ/d_{cyl} was reduced to 0.184 and the square array of cylinders was more apparent, although the shape of cylinder was not yet uniform. Finally, after 48 h annealing, the cylindrical domains registered with underlying chemical spot patterns had uniform size and shape. The value of σ/d_{cyl} for the 48 h sample was decreased from the 14 h value of 0.184 to 0.157, which was almost as small as the morphology of annealed film for 168 h ($\sigma/d_{cyl} = 0.148$). Also, the shape of semiccylinders became more and more uniform as annealing time increased.

Discussion

The combination of the experiments shown in Figures 4−6, along with the variation in morphology with progressively thicker films, shown in Figure 8, sheds light on how the polymer reconstructs its morphology as it progresses from an equilibrated state on the chemically nanopatterned surface into the bulk. As demonstrated in a variety of previous work, a chemically nanopatterned surface forces selective wetting of the chemical nanopattern by the disparate blocks of the block copolymer.[42,45,51,52] For example, as shown by Daoulas et al., the surface energy supplied by the chemical nanopattern was sufficiently strong to force a copolymer that normally has a lamellar morphology to adopt a previously unseen quadratically perforated, bicontinuous morphology when equilibrated in the presence of a chemical nanopattern of spots.[42] Application of the previous research to the work presented here results in the conclusion that the PMMA block will always wet the spots in the chemical nanopattern, and the PS will always wet the matrix area surrounding the spots. Thus, the chemically nanopatterned square array establishes in the copolymer at the surface a square array of cylinders with d_{sq} and L_{sq}. The only questions are how far this square array of cylinders progresses into the film and how the cylinders change as the distance from the substrate is increased.

As the distance from the surface is increased, the first step the copolymer takes in reconstructing its bulk morphology is to assume the preferred diameter of the bulk cylinders. As observed in the 22 nm thick film in Figure 4b, the bulk cylinder diameter was attained in a distance from the substrate that is less than half of the bulk cylinder diameter. If there was PMMA present in excess of what could be contained in the cylinders with the bulk diameter, the PMMA block spontaneously formed either semicylinders or loop cylinders. As shown in Figure 8, as the thickness of the film increased, the semicylinder and loop cylinder structures became more prevalent, until the square array was no longer visible, and sections of hexagonal arrays were present. Thus, the reconstruction of the block copolymer morphology from its equilibrated state of a square array at the substrate to a morphology similar to the bulk morphology occurred at a distance slightly more than 1.5 times the cylinder microdomain diameter. At this distance, the chemically patterned surface was ineffective at inducing the vertical cylinder morphology throughout the entire film thickness.

The degree of perfection of the replication of the chemical nanopatterning that was obtained in the block copolymer films in this work can be analyzed in terms of how closely the circle and matrix area fractions of the square array chemical nanopattern match the corresponding cross-sectional area fractions of the block copolymer cylinders and matrix in a hexagonal array. We selected the range of values for the lattice spacing and spot size in the square array based on the d_{hex} and L_{hex}. We determined the theoretical dimensions of the PS-*b*-PMMA in a square array by comparing the areas of triangle units from the vertical cylinders of a hexagonal and square array as shown Figure 11a,b. The triangle unit cell of a square array is an isosceles triangle having a right-angled vertex with L_{sq} as the lattice spacing and d_{sq} as the diameter of cylinder, similar to the definition of L_{hex} and d_{hex}. The vertices of each triangle unit locate the center of cylinders, and a triangle unit contains one-half of a cylinder cross-sectional area. The ratio of matrix area

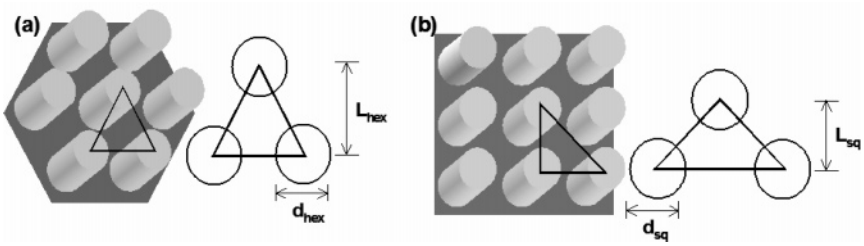

Figure 11. Schematics of vertical cylinders and triangle units of (a) a hexagonal array and (b) a square array. The diameter of cylinders and height of triangles in a hexagonal arrays are d_{hex} and L_{hex}, respectively. The diameter of cylinders and height of triangle in a square array are d_{sq} and L_{sq}, respectively.

to cylindrical area in hexagonal (A_{hex}) and square (A_{sq}) arrays is thus given by

$$A_{hex} = \frac{8L_{hex}^2}{\pi d_{hex}^2\sqrt{3}} - 1 \quad (1)$$

$$A_{sq} = \frac{8L_{sq}^2}{\pi d_{sq}^2} - 1 \quad (2)$$

The ideal dimension of cylinder-forming block copolymer in a square array can be obtained when eqs 1 and 2 are equivalent.

$$d_{sq} = \frac{3^{0.25} d_{hex}}{L_{hex}} L_{sq} \quad (3)$$

On the basis of eq 3 and the d_{hex} and L_{hex} values of 45 and 76 nm, respectively, we targeted L_{sq} values ranging from 50 to 80 nm and d_{sq} values ranging from approximately 25 to 90 nm in the lithographic patterning process.

The balance of the A_{hex} and A_{sq} can be used to achieve the square array of cylinders equilibrated with the chemical nanopattern on the surface. For example, the use of a chemical nanopattern with a balanced A_{hex} and A_{sq} caused the morphology of thin (~25 nm) films to change from the disordered collection of vertical cylinders of various sizes shown in Figure 4a to the well-ordered, square array of vertical cylinders with uniform size shown in Figure 4b. The disordered and nonuniformity of the cylinders in Figure 4a was the result of kinetic trapping of the high-M_n chains in a nonequilibrated structure, as seen before by Xu et al.[17] As in the case of Xu and co-workers, if we were able to use lower M_n copolymers, we might expect a narrower distribution of cylinder diameters on the neutral surface. However, then we would need to pattern at smaller diameters to maintain the balance of L_{sq} and d_{sq} with the preferred bulk values of d_{hex} and L_{hex}, as defined in eq 3. Instead, we selected a copolymer whose morphology dimensions matched our patterning capability but, as a result, had a high M_n that limited its ability to equilibrate on a neutral surface within our standard annealing time. Despite the high M_n, the use of the chemical nanopattern forced the copolymer into an ordered, equilibrated structure, as shown in Figure 4b. Such ordered, equilibrated structures were always achieved as long as L_{sq} and d_{sq} were in balance with the preferred bulk values of d_{hex} and L_{hex}. This result is similar to previous studies on the epitaxial assembly of lamellar structures onto striped surface patterns, which showed that as the difference between the period of stripes and the bulk lamellar period of the diblock copolymer increased, the ordering of lamellae became increasingly worse and unregistered lamellae appeared.[32,45,46] However, in the work presented here, an additional factor, the energy required to drive a hexagonal cylinder array into a square array geometry, seems to narrow or alter the parametric range over which defect free square arrays of cylinders will be formed.

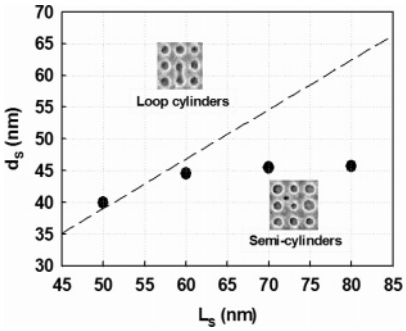

Figure 12. Plot of cylinder diameter, d_{sq}, as a function of lattice spacing, L_{sq}. Dotted line indicates the equivalent fraction of cylindrical and matrix area in the triangle units between a hexagonal and square array.

Even for 22 nm thick films, if the balance of L_{sq} and d_{sq}, with respect to L_{hex} and d_{hex}, was not maintained, when the copolymer was equilibrated with the underlying chemical nanopattern, morphologies appeared that did not match the square array chemical nanopatterning, such as the loop structures and semicylinders observable in Figures 5 and 6. The creation of loop or semicylinders on the chemical pattern of a square array was induced by the deviation of L_{sq} and d_{sq} from the theoretical dimension of cylinder-forming PS-*b*-PMMA in a square array, as outlined in eq 3. The balance of L_{sq} and d_{sq} with respect to L_{hex} and d_{hex} was used in Figure 12 to divide the parameter space of the study presented in Figure 6 into two regions: one that will lead to the formation of semicylinders and one that will lead to the formation of loop cylinders.

A simple approach to understanding the presence and quantity of semicylinders relies on a volumetric analysis of the SEM images, in which both the copolymer density and the block volume fractions are held constant. For a square array of spot patterns with $L_{sq} = 60$, 70, and 80 nm, the theoretical diameters of vertical cylinders are 46.8, 54.6, and 62.4 nm, respectively, based on eq 3. These are the diameters required to match the increase in area of the square array unit cell caused by the increase in L_{sq}. However, the cylinders on the chemical spot patterns maintained the 45 nm diameter of the underlying spot patterns, which means that excess PMMA must be present that is not included in the cylinders. Assuming that the PMMA cylinders have constant radius through the thickness of the film, simple geometry, combined with eqs 1−3, yields the fraction of PMMA not in the cylinders, $f_{MMA,xs}$, to be

$$f_{MMA,xs} = 1 - \left(\frac{L_{sq,0}}{L_{sq,xs}}\right)^2 \quad (4)$$

where $L_{sq,xs}$ is the square lattice spacing of the condition that affords excess PMMA in semicylinders and $L_{sq,0}$ is the value

of L_{sq} at which there would be no excess PMMA present. On the basis of eq 3, $L_{sq,0} = 57.7$ nm is the ideal value of lattice spacing for producing vertical cylinders having diameter of 45.0 nm in a square array.

The prediction of eq 4 was compared to the SEM image analysis of the size and quantity of semicylinders shown in Figure 6. Although eq 4 matched the qualitative trend of an increase in excess PMMA fraction with increasing L_{sq}, in all cases the prediction overestimated the fraction of excess PMMA that was observed in semicylinders. For example, for $L_{sq} = 60$ nm, eq 4 predicted an excess PMMA fraction of 6.6%, whereas the observed excess PMMA was 2%. Similarly, for $L_{sq} = 80$ nm, eq 4 predicted an excess of PMMA fraction of 47%, whereas the observed excess PMMA was 30%. Taking into account the standard deviation of the image analysis technique only compensated for half of the difference between the observed and predicted excess PMMA fraction. We can conclude that the assumption that the PMMA cylinders have constant radius through the thickness of the film is incorrect, and the primary cause of the difference was that the radii of either the cylinders or the semicylinders are not constant through the thickness of the film. From a phenomenological point of view as the L_{sq} of chemical patterns increases, there is more volume for the copolymer to fill between cylinders. There is a limited amount of PS available to fill this increased volume, so PMMA, in the form of an increased number and size of semicylinders, fills some of the increased volume between cylinders.

In the case of increasing d_{sq} for a fixed L_{sq}, shown in Figure 5, the simple relative area analysis of eq 4 does not match the trend of image analysis results for the number and size of semicylinders. This discrepancy is not surprising because the diameter of the PMMA cylinders at the top of the film was different from the diameter d_{sq} on the bottom patterned surface, so the assumption of constant cylinder diameter cannot apply. Instead of assuming a constant radius cylinder and comparing areas, the volume of the PMMA cylinders can be estimated, and then volume ratios can be compared. The volume of the cylinders can be estimated by assuming a shape for them. The simplest shape to analyze is a truncated cone, which has a volume V_{con} of

$$V_{con} = \frac{\pi(d_{sq}^{\,3} - d_{hex}^{\,3})}{12(d_{sq} - d_{hex})}\, t \tag{5}$$

where t is the thickness of the film and d_{hex} equals the diameter of the cylinder at the top of the film. It is reasonable to assume that the cylindrical PMMA domain would more likely be in the form of a catenoid, which has been predicted by Monte Carlo simulations of block copolymers in confined channels.[53] A model catenoid can be generated by fitting the catenary equation for the radius r

$$r = C\cosh\left(\frac{z}{C}\right) + r_0 \tag{6}$$

to each d_{sq} in Figure 5 to determine the constants C and r_0. Revolution of the fitted catenary described by eq 6 about the z-axis, and subsequent integration, yields the volume of the catenoid, V_{cat}, in a film with thickness t:

$$V_{cat} = \pi\frac{d_{hex}^{\,2}}{4}\, t + 2\pi\left\{\frac{C^3}{8}\sinh\left(\frac{2t}{C}\right) + C^2 r_0 \sinh\left(\frac{t}{C}\right) - \frac{C^2 t}{4} - C r_0 t\right\} \tag{7}$$

With the volume calculated for either V_{con} or V_{cat} added to the volume of the semicylinders, which was calculated from the number, diameter, and depth, as shown in Figures 5 and 7, the observed PMMA volume fraction can be estimated. This volume fraction can be compared to the volume fraction of PMMA in the copolymer, based on the respective M_n's of the blocks of the copolymer, and the densities for PS and PMMA of 1.05 and 1.19 g/cm^3, respectively.[54] As shown in Table 1, both the truncated cone and the catenoid model typically underestimated the volume fraction of PMMA in the copolymer films. Only in the case when d_{sq} was 76.8 nm did the truncated cone volume fraction prediction surpass the volume fraction determined from the densities and molecular weights of the blocks of the block copolymer. The failure of this volumetric analysis to match the observed results is most likely caused by the assumed shape for the PMMA cylinders provided by both the catenoid and truncated cone volume models being incorrect. Additionally, the model also assumes that the semicylinders are constant in diameter, which is incorrect. This analysis suggests that the cylinders may have larger diameters away from the surface or the substrate than either the catenoid or truncated cylinder geometry would predict. Another possibility is that the semicylinders have a larger diameter away from the free surface of the film. In the case of $d_{sq} = 76.8$ nm, the shape of the cylindrical domain probably lies between that of a truncated cone and a catenoid.

Although the exact shape of the PMMA microdomains cannot be determined from this model, it does suggest that the PMMA domain of PS-*b*-PMMA copolymer is expanded at the substrate interface where the spot pattern has a strong affinity for the PMMA phase and is recovered to its bulk diameter at the air interface of the film. We know from previous research that the PMMA will extend or compress its chain configuration when it is equilibrated in the presence of the chemical nanopattern so that it wets the chemical nanopattern.[42,50,51] However, this distortion of the PMMA cylinders still did not provide sufficient volume for the PMMA in the film. The copolymer film on the substrate with smaller d_{sq}, such as that shown in Figure 5a, had a smaller area on the substrate to accommodate the PMMA phase and therefore was more likely to create more volume for PMMA by forming PMMA semicylinders. It is important to note that the thickness of these 22 nm films is only half of the 45 nm preferred diameter of the bulk cylindrical copolymer domains, so the polymer has the ability to form with more of the PMMA material coating the surface when the spot size is larger.

The fact that the larger spot size created copolymer films with fewer semicylinder defects in the array has technological implications for the use of these copolymer films in lithographic applications. The larger spot diameter of chemical patterns, compared to the diameter of the bulk cylinders, was still effective for producing vertically oriented cylindrical domains of a square array. Smaller spot patterns, however, were ineffective at forming a square array of vertical cylinders on the chemical pattern. When $L_{sq} = 60$ nm, cylinder-forming PS-*b*-PMMA thin films on spot patterns smaller than $d_{sq} = 40$ nm exhibited parallel and perpendicular orientation of cylindrical domains that were randomly ordered over the whole region of chemical pattern.

Table 1. Estimated PMMA Volume Fractions

	volume fraction estimate method[a]		
d_{sq} (nm)	block volume	truncated cone[b]	catenoid[b]
52.6	0.30	0.21	0.20
60.5	0.30	0.24	0.21
68.6	0.30	0.27	0.24
76.8	0.30	0.31	0.26

[a] Estimation of PMMA volume fractions was based on relative block volumes in the block copolymer as well as cylinder domain geometries based on a truncated cone model and a catenoid model. [b] The truncated cone and catenoid models include the PMMA present in semicylinders.

Just as semicylinders were likely to form as L_{sq} increased to a length that was out of balance with d_{sq} as defined in eq 3, loop cylinders were likely to form as L_{sq} decreased from a length that was in balance with d_{sq}. According to eq 3, the theoretical diameter of vertically oriented cylinders should be 39.0 nm when $L_{sq} = 50$ nm. Although the diameter of the spot patterns used in this study was 45.0 nm, the same as the natural size of copolymer, assembly of cylinder-forming PS-*b*-PMMA on this chemical pattern produced much smaller diameter vertical cylinders (ca. 40 nm) at the free surface of copolymer film. The smaller cylinder diameter may imply that the concentration of diblock copolymer chains available for the formation of cylindrical domains was decreased to diminish the size of copolymer domains. Therefore, some of the diblock copolymer chains were employed to form vertical cylinders on chemical spot patterns, and the rest of them produced parallel cylinders connecting two cylinders on the chemical spot patterns. As a result, loop structures were created on chemical spot patterns in square arrays with $L_{sq} = 50$ nm.

The copolymer film shown in Figure 6d was far enough out of balance in terms of eq 3 that loop cylinders, semicylinders, and loop cylinder and semicylinder combinations were present. The red circles in Figure 6d show the underlying substrate pattern and reveal that some of the loop cylinders made a diagonal across the square array unit cell, which would connect with a semicylinder if it were present in the center of the square array unit cell. The substrate pattern of the film shown in Figure 6d had L_{sq} and d_{sq} of 80 nm and 45 nm, respectively. To maintain the balance established in eq 3, the d_{sq} should have been 62 nm. The cylindrical PMMA microdomains could not increase to that size, and instead, a variety of structures were formed that did not match the underlying square array chemical nanopattern.

One undercurrent of all of these morphological observations was the tendency of the PMMA domains of the thin copolymer films to reach their preferred bulk cylinder diameters in a very short distance from the substrate surface. The larger spot sizes used for the films shown in Figures 4 and 5 did not translate to equally large spot sizes on the top surface of the film. Similarly, even though larger lattice spacings in Figure 6 would maintain the area ratio established in eq 3, the cylinder diameters remained at 45 nm. Only the films cast on small L_{sq}, such as that shown in Figure 6a in which $L_{sq} = 50$ nm, deviated from this trend, and in that case it was to a smaller diameter.

Conclusion

This work demonstrates that a well-ordered square array of cylinders can be formed on a surface from a block copolymer that typically consists of a hexagonal array of cylinders, thereby providing an extension of the capabilities of directed assembly of block copolymers on chemically nanopatterned substrates. A chemically nanopatterned square array of dots on the substrate induced the block copolymer to form perpendicularly oriented cylinders in a square array. When the dimension of the diblock copolymer domains were incommensurate with that of the chemical surface pattern, unprecedented structures of PMMA phase, such as loop and semicylinder structures, were spontaneously formed to compensate for the mismatch. Additionally, we observed that the cylinder phase of the block copolymer quickly reconstructs its preferred bulk cylinder diameter as the polymer moves away from the chemically nanopatterned surface. The reconstruction of the bulk cylinder dimensions occurred at distance from the substrate equal to half the bulk cylinder diameter. At a distance from the substrate of 1.5 times the bulk cylinder diameter, the effect of the chemically nanopatterned surface is no longer apparent. The rapid reconstruction of the bulk morphology as the copolymer moves away from the surface occurs due to the limited interactions between the surface pattern and the thin film of block copolymers.

For future lithography needs, thin films on the order of the thicknesses used in this study are required. Therefore, the processes presented in this work can still be applied to the directed assembly of block copolymers on chemically nanopatterned substrates because the square arrays of cylinders are maintained over film thicknesses that are sufficiently large for future lithographic needs. More generally, the distinct advantages of this work are that the capability of block copolymer lithography can be extended by using chemically patterned surfaces different than the preferred bulk morphology of block copolymers.

Acknowledgment. Exposure was performed on the X-ray interference at the Swiss Light Source, part of the Paul Scherrer Institut in Villigen Switzerland. This work was supported by the Semiconductor Research Corporation (SRC) (2005-MJ-985) and the National Secience Foundation through the Nanoscale Science and Engineering Center (DMR-0425880). This work was based in part upon research conducted at the Synchrotron Radiation Center, University of Wisconsin—Madison, which is supported by the NSF under Award DMR-0084402.

References and Notes

(1) Knoll, A.; Horvat, A.; Lyakhova, K. S.; Krausch, G.; Sevink, G. J. A.; Zvelindovsky, A. V.; Magerle, R. *Phys. Rev. Lett.* **2002**, *89*, 035501.
(2) Shin, K.; Leach, K. A.; Goldbach, J. T.; Kim, D. H.; Jho, J. Y.; Tuominen, M.; Hawker, C. J.; Russell, T. P. *Nano Lett.* **2002**, *2*, 933.
(3) Thurn-Albrecht, T.; Steiner, R.; DeRouchey, J.; Stafford, C. M.; Huang, E.; Bal, M.; Tuominen, M.; Hawker, C. J.; Russell, T. P. *Adv. Mater.* **2000**, *12*, 1138.
(4) Xiao, S. G.; Yang, X. M.; Edwards, E. W.; La, Y. H.; Nealey, P. F. *Nanotechnology* **2005**, *16*, S324.
(5) Chang, L.-W.; Wong, H.-S. P. *Proc. SPIE* **2006**, *6156*, 615611-1.
(6) Zhang, Q. L.; Xu, T.; Butterfield, D.; Misner, M. J.; Ryu, D. Y.; Emrick, T.; Russell, T. P. *Nano Lett.* **2005**, *5*, 357.
(7) Black, C. T.; Guarini, K. W.; Milkove, K. R.; Baker, S. M.; Russell, T. P.; Tuominen, M. T. *Appl. Phys. Lett.* **2001**, *79*, 409.
(8) Black, C. T.; Guarini, K. W.; Zhang, Y.; Kim, H. J.; Benedict, J.; Sikorski, E.; Babich, I. V.; Milkove, K. R. *IEEE Electron Device Lett.* **2004**, *25*, 622.
(9) Gratt, J. A.; Cohen, R. E. *J. Appl. Polym. Sci.* **2004**, *91*, 3362.
(10) Guarini, K. W.; Black, C. T.; Milkove, K. R.; Sandstrom, R. L. *J. Vac. Sci. Technol. B* **2001**, *19*, 2784.
(11) Shibauchi, T.; Krusin-Elbaum, L.; Gignac, L.; Black, C. T.; Thurn-Albrecht, T.; Russell, T. P.; Schotter, J.; Kastle, G. A.; Emley, N.; Tuominen, M. T. *J. Magn. Magn. Mater.* **2001**, *226*, 1553.
(12) Olayo-Valles, R.; Lund, M. S.; Leighton, C.; Hillmyer, M. A. *J. Mater. Chem.* **2004**, *14*, 2729.
(13) Thurn-Albrecht, T.; Schotter, J.; Kastle, C. A.; Emley, N.; Shibauchi, T.; Krusin-Elbaum, L.; Guarini, K.; Black, C. T.; Tuominen, M. T.; Russell, T. P. *Science* **2000**, *290*, 2126.
(14) Huang, E.; Rockford, L.; Russell, T. P.; Hawker, C. J. *Nature (London)* **1998**, *395*, 757.

(15) Huang, E.; Russell, T. P.; Harrison, C.; Chaikin, P. M.; Register, R. A.; Hawker, C. J.; Mays, J. *Macromolecules* **1998**, *31*, 7641.
(16) In, I.; La, Y. H.; Park, S. M.; Nealey, P. F.; Gopalan, P. *Langmuir* **2006**, *22*, 7855.
(17) Xu, T.; Kim, H. C.; DeRouchey, J.; Seney, C.; Levesque, C.; Martin, P.; Stafford, C. M.; Russell, T. P. *Polymer* **2001**, *42*, 9091.
(18) Yang, X. M.; Xiao, S. G.; Liu, C.; Pelhos, K.; Minor, K. *J. Vac. Sci. Technol. B* **2004**, *22*, 3331.
(19) Lin, Z. Q.; Kim, D. H.; Wu, X. D.; Boosahda, L.; Stone, D.; LaRose, L.; Russell, T. P. *Adv. Mater.* **2002**, *14*, 1373.
(20) Ho, R. M.; Tseng, W. H.; Fan, H. W.; Chiang, Y. W.; Lin, C. C.; Ko, B. T.; Huang, B. H. *Polymer* **2005**, *46*, 9362.
(21) Sidorenko, A.; Tokarev, I.; Minko, S.; Stamm, M. *J. Am. Chem. Soc.* **2003**, *125*, 12211.
(22) Xu, T.; Zvelindovsky, A. V.; Sevink, G. J. A.; Lyakhova, K. S.; Jinnai, H.; Russell, T. P. *Macromolecules* **2005**, *38*, 10788.
(23) Park, C.; De Rosa, C.; Lotz, B.; Fetters, L. J.; Thomas, E. L. *Macromol. Chem. Phys.* **2003**, *204*, 1514.
(24) De Rosa, C.; Park, C.; Thomas, E. L.; Lotz, B. *Nature (London)* **2000**, *405*, 433−437.
(25) Black, C. T.; Guarini, K. W. *J. Polym. Sci., Part A: Polym. Chem.* **2004**, *42*, 1970.
(26) Kim, S. H.; Misner, M. J.; Russell, T. P. *Adv. Mater.* **2004**, *16*, 2119.
(27) Kim, G.; Libera, M. *Macromolecules* **1998**, *31*, 2569.
(28) Kim, S. H.; Misner, M. J.; Xu, T.; Kimura, M.; Russell, T. P. *Adv. Mater.* **2004**, *16*, 226.
(29) Sundrani, D.; Sibener, S. J. *Macromolecules* **2002**, *35*, 8531.
(30) Black, C. T.; Bezencenet, O. *IEEE Trans. Nanotechnol.* **2004**, *3*, 412.
(31) Cheng, J. Y.; Ross, C. A.; Smith, H. I.; Thomas, E. L. *Adv. Mater.* **2006**, *18*, 2505.
(32) Edwards, E. W.; Montague, M. F.; Solak, H. H.; Hawker, C. J.; Nealey, P. F. *Adv. Mater.* **2004**, *16*, 1315.
(33) Wang, Q.; Nealey, P. F.; de Pablo, J. J. *Macromolecules* **2003**, *36*, 1731.
(34) In Directed Self Assembly of Materials for Patterning Workshop, Madison, WI, June 16, 2005, Semiconductor Research Corporation/ National Nanotechnology Initiative, Madison, WI.
(35) Stocker, W.; Beckmann, J.; Stadler, R.; Rabe, J. P. *Macromolecules* **1996**, *29*, 7502.
(36) Rehse, N.; Knoll, A.; Magerle, R.; Krausch, G. *Macromolecules* **2003**, *36*, 3261.
(37) Wang, Q.; Nealey, P. F.; de Pablo, J. J. *Macromolecules* **2001**, *34*, 3458.
(38) Tsarkova, L.; Horvat, A.; Krausch, G.; Zvelindovsky, A. V.; Sevink, G. J. A.; Magerle, R. *Langmuir* **2006**, *22*, 8089.
(39) Konrad, M.; Knoll, A.; Krausch, G.; Magerle, R. *Macromolecules* **2000**, *33*, 5518.
(40) Park, I.; Park, S.; Park, H. W.; Chang, T.; Yang, H. C.; Ryu, C. Y. *Macromolecules* **2006**, *39*, 315.
(41) Knoll, A.; Magerle, R.; Krausch, G. *J. Chem. Phys.* **2004**, *120*, 1105.
(42) Daoulas, K. C.; Muller, M.; Stoykovich, M. P.; Park, S. M.; Papakonstantopoulos, Y. J.; de Pablo, J. J.; Nealey, P. F.; Solak, H. H. *Phys. Rev. Lett.* **2006**, *96*, 036104.
(43) Mansky, P.; Liu, Y.; Huang, E.; Russell, T. P.; Hawker, C. *Science* **1997**, *275*, 1458.
(44) Huang, E.; Pruzinsky, S.; Russell, T. P.; Mays, J.; Hawker, C. J. *Macromolecules* **1999**, *32*, 5299.
(45) Edwards, E. W.; Stoykovich, M. P.; Muller, M.; Solak, H. H.; De Pablo, J. J.; Nealey, P. F. *J. Polym. Sci., Part B: Polym. Phys.* **2005**, *43*, 3444.
(46) Edwards, E. W.; Stoykovich, M. P.; Nealey, P. F.; Solak, H. H. *J. Vac. Sci. Technol. B* **2006**, *24*, 340.
(47) Edwards, E. W.; Stoykovich, M. P.; Solak, H. H.; Nealey, P. F. *Macromolecules* **2006**, *39*, 3598.
(48) Solak, H. H. *J. Phys. D: Appl. Phys.* **2006**, *39*, R171.
(49) Guarini, K. W.; Black, C. T.; Yeuing, S. H. I. *Adv. Mater.* **2002**, *14*, 1290.
(50) Daoulas, K. C.; Muller, M.; Stoykovich, M. P.; Papakonstantopoulos, Y. J.; De Pablo, J. J.; Nealey, P. F.; Park, S. M.; Solak, H. H. *J. Polym. Sci., Part B: Polym. Phys.* **2006**, *44*, 2589.
(51) Stoykovich, M. P.; Edwards, E. W.; Solak, H. H.; Nealey, P. F. *Phys. Rev. Lett.* **2006**, *97*, 147802.
(52) Daoulas, K. C.; Muller, M.; de Pablo, J. J.; Nealey, P. F.; Smith, G. D. *Soft Matter* **2006**, *2*, 573.
(53) Chen, P.; He, X. H.; Liang, H. J. *J. Chem. Phys.* **2006**, *124*, 104906.
(54) Brandrup, J.; Immergut, E. H. *Polymer Handbook*, 3rd ed.; John Wiley & Sons: New York, 1989.

MA0702344